Soft Matter

PAPER

View Article Online
View Journal | View Issue

Cite this: *Soft Matter*, 2024, **20**, 2804

Analysis of the peel structure of different *Citrus* spp. *via* light microscopy, SEM and µCT with manual and automatic segmentation†

Maximilian Jentzsch, *[ab] Vanessa Albiez,[a] Thalia C. Kardamakis [a] and Thomas Speck *[abcd]

The peels of lime, lemon, pomelo and citron are investigated at macroscopic and microscopic level. The structural composition of the peels is compared and properties such as peel thickness, proportion of flavedo, density and proportion of intercellular spaces are determined. µCT images are used to visualize vascular bundles and oil glands. SEM images provide information about the appearance of the cellular tissue in the outer flavedo and inner albedo. The proportion of intercellular spaces is quantitatively determined by manual and software-assisted analysis (ilastik). While there are macroscopic differences in the fruits, they differ only slightly in the orientation of the vascular bundles and the arrangement of the oil glands. However, in peel thickness and flavedo thickness, the fruit peels differ significantly from each other. There are no significant differences between the two analysis methods used, although the use of ilastik is preferred due to time reduction of up to 70%. The large amount of intercellular spaces in the albedo but also the denser flavedo both have a mechanical protective function to prevent damage to the fruit. In addition, the entire peel structure is mechanically reinforced by vascular bundles. This combination of penetration protection (flavedo) and energy dissipation (albedo) makes *Citrus* spp. peels a promising inspiration for technical material systems.

Received 8th November 2023,
Accepted 25th February 2024

DOI: 10.1039/d3sm01511d

rsc.li/soft-matter-journal

1. Introduction

The peels of citrus fruits, and especially of the pomelo, are characterized by specific mechanical properties allowing for high energy dissipation during impact. Whether it is high energy dissipation,[1–4] (nearly auxetic) lateral compression behavior[3,5–7] or other mechanical properties[3,4,6,8] that indicate their excellent damping properties. Therefore, the peels of citrus fruits can generally act as an inspiration for biologically inspired technical material systems and lightweight structures.[3,4,9–11]

Citrus peels typically consist of exocarp (flavedo), mesocarp (albedo), and endocarp[2,12,13] (Fig. 1). However, the peels of individual species differ in some characteristics such as color and peel thickness.[2,7,14,15] The flavedo, which consists of epidermis, cuticle, and parenchymatous cell tissues, is characterized by its densely packed cells and the oil glands within.[2,13] The albedo makes up a large part of the peel and is a less dense arranged tissue with parenchymatic cells that contains more intercellular spaces than the flavedo.[2,12,13] In addition, lignified vascular bundles run through the albedo and through the flavedo.[1] The endocarp is a thin inner layer and encloses the pulp of the fruit with the seeds.[2]

In this study, the structure of the peel of various citrus fruits is visualized and studied in more detail with the aim to

[a] *Plant Biomechanics Group, Botanic Garden, Faculty of Biology, University of Freiburg, Schänzlestraße 1, D-79104 Freiburg, Germany. E-mail: Maximilian.jentzsch@biologie.uni-freiburg.de, Thomas.Speck@biologie.uni-freiburg.de*
[b] *Cluster of Excellence livMatS @ FIT, Georges-Köhler-Allee 105, D-79110 Freiburg, Germany*
[c] *Freiburg Materials Research Center (FMF), Stefan-Meier-Straße 21, D-79104 Freiburg, Germany*
[d] *Freiburg Center for Interactive Materials and Bioinspired Technologies (FIT), Georges-Köhler-Allee 105, D-79110 Freiburg, Germany*

† Electronic supplementary information (ESI) available. See DOI: https://doi.org/10.1039/d3sm01511d

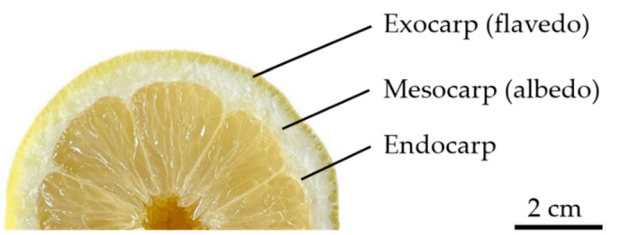

Fig. 1 Equatorial cross section of a lemon (*Citrus* × *limon*) visualizing the general peel structure of citrus fruits and their fruit peels.

contribute to a better understanding of the form–structure–function relation in this highly damping material system. For the first time, we have used a combination of methods that allows us to quantitatively analyse the arrangement of cells and vascular bundles in intact citrus fruit peels in 3D, which is a prerequisite for a successful biomimetic transfer. The fruit peels are examined using different imaging techniques (light microscopy, SEM, μCT) at both macroscopic and microscopic level. Thus, light- and scanning electron microscopy (SEM) is used to examine the cell tissue and cell arrangement. Furthermore, microcomputed tomography (μCT) is used to visualize the arrangement of the oil glands and the orientation of the vascular bundles. X-Ray computed tomography scanning is a way to present a 3D visualization of objects in a non or less-destructive manner.[16,17] It is also known as high-resolution X-ray computed tomography (HRXCT) as it can have resolutions at sub-micron levels (50 μm–325 nm).[16,17] The term microcomputed tomography or μCT is used in this study.

The varying intensity of intercellular spaces, which differ between citrus species, has so far been determined in time-consuming manual measurements. This is due to the mainly inhomogeneous biological tissue and a weak contrast between cell tissue, liquids and intercellular spaces. The manual, 2-dimensional evaluation is often subjective and difficult to reproduce, but above all very time-consuming. For a 3-dimensional analysis of *e.g.* CT-scans the software MORPHO+, for example, uses a watershed algorithm and subsequently color-coded analysis according to the volume virtually separated.[16,18] There is also a variety of other software tools for 2-dimensional and 3-dimensional segmentation such as Fiji Weka,[19] SuRVos,[20] or FastER.[21] In this study, intercellular spaces are determined not only manually but also using the machine-learning based image analysis software ilastik (open source project). ilastik is an open source project that allows users without (much) expertise in image processing to perform segmentation and classification.[18,22] For classification, ilastik uses a random forest classifier.[23,24] The classifier learns from the users' input, which trains it in an interface that is similar to the interface of the Microsoft Paint software.[18] It proposes real-time feedback and a convenient interface.[18] New labels are used to fine-tune the classifier interactively.[18,24] Once a classifier has been trained, it can be used to process a whole data set.[18] Furthermore, ilastik allows volumes to be segmented into larger voxels using a watershed algorithm.[22]

2. Materials and methods

2.1 Plant material

For the analysis of the peel, fruits of *Citrus* × *latifolia* (lime), *Citrus* × *limon* (lemon), *Citrus maxima* (pomelo), and *Citrus medica* (citron) were used (Fig. 2). For the exact origin and variety, see Table 1. Lime fruits are typically in an immature state (green epidermis). Accordingly, they were studied in this state. In the following, the fruits and peels are referred to using the trivial name. Only fruits without external defects were used. The fruits were purchased from local suppliers, and care was taken to ensure that the fruits were untreated and undamaged by external inspection.

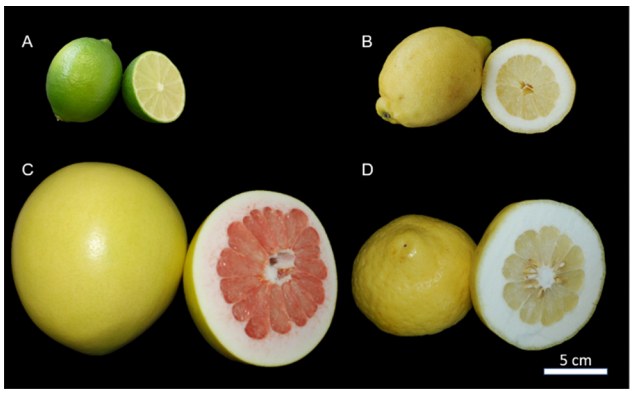

Fig. 2 Analyzed citrus fruits with their peel and pulp; (A) lime (*Citrus* × *latifolia*); (B) lemon (*Citrus* × *limon*); (C) pomelo (*Citrus maxima*) and (D) citron (*Citrus medica*).

Table 1 Analyzed citrus fruits within this study

Species	Variety	Trivial name	Number of fruits	Origin of fruits
C. × *latifolia*	Persian lime	Lime	8	Vietnam
C. × *limon*	Verna	Lemon	6	Spain
C. maxima	Red honey pomelo	Pomelo	8	China
C. medica	Nasone	Citron	8	Italy

2.2 Morphological measurement

The fruits were cut equatorially, and one image was taken per fruit. The images were measured using ImageJ/Fiji software (version 1.52a) so that the proportion of peel, in relation to the cross-sectional area of the fruit, could be determined. The density of the peels was determined using 10 cylindrical samples taken from the equatorial area of each fruit. The samples were made using a cork borer with an inner diameter of 15.31 ± 0.03 mm. The weight of the samples was measured using a fine scale (±0.1 mg). To measure the samples' height, a caliper (±0.03 mm) was used. For the analysis of the intercellular spaces, thin sections of the fruit skin were prepared (see Section 2.3 Thin sections). Images of the thin sections were taken for analysis. The images of the thin sections were also used to determine the thickness of the flavedo. However, the transition from flavedo to albedo is gradual. Therefore, the distance between the epidermis and the nearest larger intercellular space, that is not between two oil glands or adjacent to a vascular bundle, was chosen and classified as flavedo thickness.

2.3 Thin sections

In order to be able to determine the relative proportion of intercellular spaces in the peel, 10 cross-sectional thin sections (3–5 μm) were prepared from 6–8 fruits of each species. First, cuboidal samples were cut from the equatorial region of the fruit with a scalpel. A razor blade was used to cut off the pulp. Then, the samples were preserved for 3 d in formalin-acetic acid alcohol (FAA: 70% ethanol, acetic acid, 37% formaldehyde

solution (90 : 5 : 5)). For dehydration, samples were placed in 70% isopropanol for 24 h, followed by 2 h in 90% isopropanol and 1.5 h in 100% isopropanol. Thereafter, the samples were fixated and embedded in a polymer (Technovit 7100) (Kulzer GmbH, Hanau, Germany). For this purpose, the samples were placed in a solution of Technovit 7100 and 100% isopropanol for 8 h for pre-infiltration (1 : 1). Subsequently, the samples were stored for another 8 h in an infiltration solution of Technovit 7100 (100 ml) and Hardener I (1 g). Finally, the samples are placed in a mold for polymerization and placed in a solution of 30 ml of infiltration solution and 1.5 ml of Hardener II for another 8 h. The polymerized samples are placed in a mold for polymerization. The polymerized samples are stuck onto a plastic cube and can then be cut into thin sections of 3–5 μm thickness using a rotary microscope (Leica Mikrosysteme Vertrieb GmbH, Wetzlar, Germany). The thin sections are stained with toluidine blue (0.05%) and covered with Entallan (Merck KGaA, Darmstadt, Germany). Images were captured using a light microscope (BX61, Olympus, Hamburg, Germany) with a digital camera (DP71, Olympus, Hamburg, Germany) using Cell P software (version 2.6 (build 1200)). The images were used for manual and software-based determination of the intercellular spaces.

2.4 Intercellular spaces

The thin section images of the peels were used to determine the proportion of intercellular spaces. A 2 mm wide area with individual length (from epidermis to endodermis) of the section was selected from all images and saved as 8-bits in HDF5 format. The section was selected to reduce the amount of data. The selected area was segmented and divided into cells and intercellular spaces. Segmentation was performed using two different methods. The first method included the areas being manually segmented using the lasso function of the ImageJ/Fiji software (version 2.1.0/1.53c). For the second method, the areas were segmented using ilastik (version 1.3.2), a machine-learning-based image analysis software. Detailed instructions on the procedure can be found in ESI.† The segmented images were then further processed with the image software ImageJ/Fiji using the threshold function to measure the relative proportion of intercellular spaces of the citrus fruit peel.

2.5 μCT and SEM imaging of peel samples

To improve the contrast due to the high liquid content of the samples, the samples had to be critically point dried before applying an imaging technique (SEM or CT-imaging).[25] For preservation, the samples were placed in a 30%, 40%, 50%, 60%, 70%, 80%, 90% and 100% ethanol series for one day each. The samples were dried using a critical point dryer (CPD 030, Bal-Tec AG, Balzers, Lichtenstein). After the samples have been dried, they could be scanned using the μCT.

2.5.1 μCT imaging. For characterization of the peel structure, μCT images were obtained using the μCT (Skyscan 1272, Bruker, Kontich, Belgium), the Skyscan 1272 μCT software (version 1.1.10), NRecon software (version 1.6.10.1) for reconstruction and CTVox software (version 3.0.0 r1122) for visualization. In addition to the qualitative distribution of the vascular bundles within the peel, the oil glands were also visualized. The segmentation of the vascular bundles was done with Avizo software (version 2020.2).

2.5.2 SEM imaging. In order to visualize the cell structure and cell arrangement, these were imaged using a scanning electron microscope (LEO 435 V, LEO Electron Microscopy Inc., Thornwood, USA) at different magnifications in micrometer scale. Samples for SEM imaging were obtained from the equatorial fruit zone. These peel sections were taken from the area of the epidermis to the border of peel and pulp. Before the samples were used, they were critically point dried and coated with gold using a sputter coater (108 auto, Cressington Scientific Instruments UK, Watford, UK) to obtain conductivity.

2.6 Statistics

Statistical analysis was performed using R software (version 4.0.0) and R-Studio (version 1.2.5042).[26] The generated data sets were tested for normal distribution using the Shapiro test. If the data were normally distributed, the mean and standard deviation (SD) were calculated. If the data was not normally distributed, the median and interquartile range (IQR) were reported. Before using the statistical tests appropriate for normally distributed data, a Levene test was used to check for homogeneity of variances. The data sets were then divided into ≤ 2 and > 2 groups according to the number of groups. For ≤ 2 groups, a *t*-test was used for independent data sets. For dependent data sets, the 'paired *t*-test' was used. For independent, normally distributed data sets with more than 2 groups, ANOVA was used to test for significant differences. For dependent data sets, 'repeated measures ANOVA' was used. If the data sets were not normally distributed, the Wilcoxon–Mann–Whitney test was performed for a number of groups ≤ 2 for dependent data and the 'paired Wilcoxon test' was performed for independent data (with holm correction). When the non-normally distributed data set consisted of more than 2 groups, the Kruskal–Wallis test was used for dependent data and the 'repeated measures Kruskal–Wallis test' was used for independent data. If the probability of error was less than 5% ($p < 0.05 \geq 0.01$), the result was considered significant and marked with *. If the probability of error was less than 1% ($p < 0.01 \geq 0.001$), the result was called very significant, and if it was less than 0.5% ($p < 0.001$), the result was called highly significant. The probability of error of less than 1% was marked with ** and of less than 0.1% with ***. In the case of non-significantly different results, this was marked by n.s.

3. Results

3.1 Morphological results

The macroscopic analysis of the fruits shows that there is a highly significant difference ($p > 0.001$) between most of the fruits regarding their relative peel proportion (Table 2). However, no significant difference between lemon and pomelo could be found ($p > 0.05$). The highest peel proportion is found

Table 2 Morphological results of *Citrus* spp. For normally distributed data mean and standard deviation are calculated (mean ± SD). Non-normally distributed data are displayed by median and interquartile range (median(IQR)). *n* represents the number of samples. The significant differences of the parameters between the species are represented by the alphabetical codes

Species	Peel proportion [%]	Peel density [kg m^{-3}]	Peel thickness [mm]	Flavedo thickness [mm]
Lime	22.78(2.63) (n = 12); ABC	997.67 ± 74.27 (n = 17); ABC	2.77 ± 0.42 (n = 17); ABC	0.92 ± 0.17 (n = 10); ABC
Lemon	37.63(9.13) (n = 20); AD	831.79 ± 40.14 (n = 10); ADE	7.64 ± 0.95 (n = 10); ADE	2.60 ± 0.90 (n = 10); AD
Pomelo	46.93(13.66) (n = 10); BE	417.72 ± 60.02 (n = 17); BD	18.37 ± 5.46 (n = 17); BD	0.22 ± 0.07 (n = 10); BDE
Citron	65.68(4.55) (n = 15); CDE	416.63 ± 22.62 (n = 10), CE	19.81 ± 1.54 (n = 10); CE	2.97 ± 0.51 (n = 10); CE

in citron (65.68%), whereas lime shows the lowest peel proportion (22.78%). In terms of peel density, the reverse is observed with respect to the peel proportion. Thus, lime has the significantly highest density (997.67 kg m^{-3}) ($p > 0.001$) and citron and pomelo show the lowest density with 416.63 and 417.72 kg m^{-3}. Peel thickness behaves similarly to the peel proportion. The thickest peels are found in pomelo and citron that do not differ significantly ($p > 0.05$), and the thinnest in lime. The thickest flavedos are found in citron (2.97 mm) and in lemon (2.60 mm) that do not differ significantly ($p > 0.05$). The flavedo thicknesses of the other species are highly significantly lower ($p < 0.001$). It is remarkable that the flavedo is the thinnest in pomelo the largest citrus fruit (0.22 mm). Comparing the flavedo thickness in relation to the peel thickness, it accounts for about 33% for lime and lemon, for citron approximately 15% and for pomelo about 1%.

3.2 CT imaging

The µCT images of lemon are characteristic for the µCT scans of all tested fruits (µCT images of the peel of lemon, pomelo and citron and also videos of the scans of lemon and pomelo can be found in ESI†). The images clearly show that the peel of citrus fruits mainly consists of epidermis, oil glands, vascular bundles and parenchymatic tissue cells (flavedo, albedo and endodermis) (Fig. 3). While the oil glands are found exclusively in the outer tissue (flavedo), the vascular bundles run predominantly radial from pulp to epidermis in the entire peel. The segmentation of the vascular bundles within the peel illustrates the orientation of the vascular bundles within the peel. In addition, the vascular bundles branch with increasing frequency as they approach the epidermis. With increasing branching, however, the diameter of the vascular bundles decreases so that the volumetric contribution remains nearly constant.

3.3 SEM imaging

The SEM images of citron are characteristic for all tested species (SEM images of lime and lemon, Fig. S3, ESI†). They illustrate that the tissues of flavedo (Fig. 4A and C) and albedo (Fig. 4B and D) are different. Both tissue types are found in the peel of all four citrus species, but in varying thickness and proportion. The cells of the outer flavedo are larger and more densely arranged than the albedo cells. Cells in both tissues have cell wall thicknesses of 3–5 µm. The SEM images of the albedo tissue also reveal the increase in intercellular spaces in the tissue compared to the flavedo tissue.

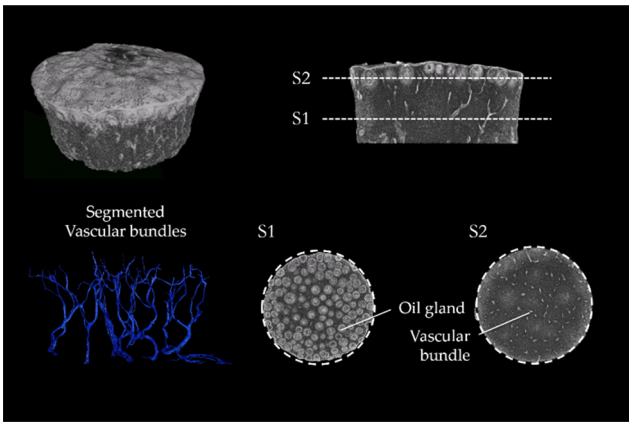

Fig. 3 *Citrus* x *limon* var. verna (lemon): µCT scan of a critical point dried lemon peel sample with a diameter of 1.5 cm. The scan visualizes the distribution of oil glands (S1) and vascular bundles (S2) in the peel. The segmentation of vascular bundles shows the branching and primary orientation of the vascular bundles.

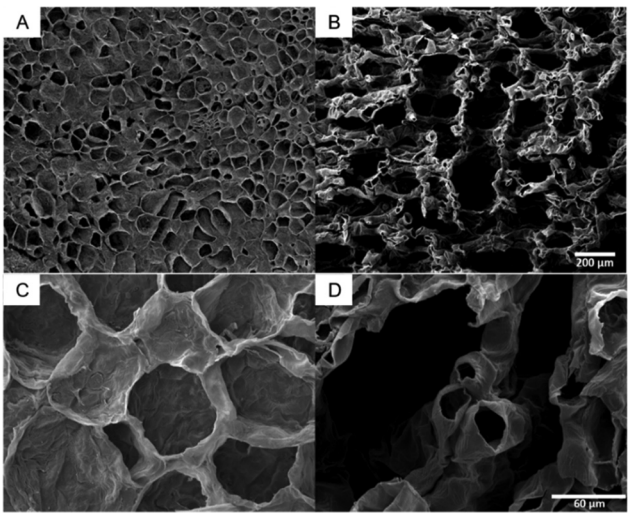

Fig. 4 SEM images of the peel tissue of citron. Broader overview of the outer flavedo (A) and the inner albedo (B) (same magnification for A and B). Higher magnification of flavedo (C) and albedo cells (D) (same magnification for C and D).

3.4 Intercellular spaces of the peel of *Citrus* spp.

To compare the validity of the determination of the intercellular spaces using ilastik software, the 10 thin sections of lemon and lime were measured both manually and with ilastik software (Fig. 5A). The results showed that the proportion of intercellular spaces was not significantly different ($p > 0.05$) for lemon (19.37% ± 4.20% manually, 17.80% ± 2.32% ilastik) and for lime (8.30% ± 1.46% manually, 8.76% ± 2.67% ilastik).

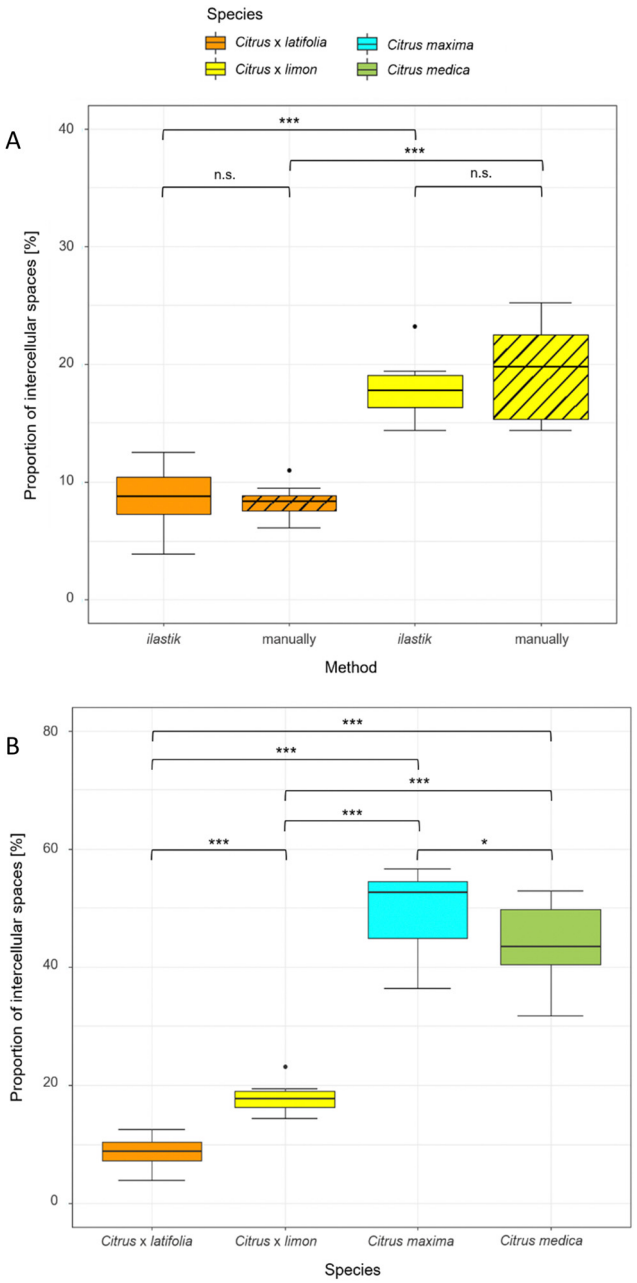

Fig. 5 Proportion of intercellular spaces for *Citrus* spp. peels (median with interquartile range). (A) Comparison of manual measurements and ilastik method for the determination of intercellular spaces. Only the images of two species (lime and lemon) were used for the comparison. (B) Proportion of intercellular spaces for *Citrus* spp. using ilastik software for segmentation. 10 thin sections were analyzed for each species.

Furthermore, this comparison shows that lemon has a highly significantly larger ($p < 0.001$) proportion of intercellular spaces than lime in both manual and ilastik measurements.

Using ilastik software, the relative proportion of intercellular spaces was determined for all four fruit peels (lime, lemon, pomelo and citron) from 10 thin sections (Fig. 5B). The pomelo has with 49.65% ± 6.82% the highest proportion of intercellular spaces. The pomelo is followed by citron which has significantly less intercellular spaces with 43.72% ± 6.90% ($p < 0.05$). Lemon and lime, which are highly significantly different from each other ($p < 0.001$), are also highly significantly different from pomelo and citron with 17.80% ± 2.32% (lemon) and 8.76% ± 2.67% (lime) intercellular spaces ($p < 0.001$).

4. Discussion

In this study, macroscopic observations and different imaging techniques (light microscopy, SEM, µCT) on a microscopic level provide a detailed insight into the structural composition of various citrus fruits.

The fruits of the four species studied (lime, lemon, pomelo and citron) differ visually in size and color (Fig. 2). In addition, the peel proportion in relation to the whole fruit differs highly significantly from each other ($p < 0.005$) (Section 3.1 Morphological results). The largest fruits (citron and pomelo) have the largest peel proportion with the lowest density and the lowest relative flavedo thickness (Section 3.1 Morphological results).

Selective breeding has been used to reduce the proportion of peel in favor of pulp.[27,28] Therefore, species that have evolved through intensive breeding show significantly less peel than less 'high' cultivated species. Moreover, if the ontogeny of citrus fruits is taken into account, a denser peel tissue in fruits with lower relative peel content is substantiated. Initially, cell multiplication in the ovule wall is approximately uniform. In young fruits, the cells of the pericarp (peel) are thin-walled. During further ontogeny, the exocarp, mesocarp, and endocarp differentiate in the pericarp.[12] In the first stage of growth the increase in fruit size is mainly due to the increasing thickness of the peel.[29] Thus, the ovary wall develops into the tissue, which differentiates into flavedo and albedo, and the juice sacs form in the fruiting segments. The second growth stage, which is a period of rapid growth, is distinguished on the basis of and characterized by cell enlargement. Here, the greatest increase in size is due to the growth of the pulp and the juice concentration also increases. The peel reaches its maximum thickness at the beginning of this stage and then becomes thinner and the pulp continues to increase in size. During stage 2, there are marked anatomical changes in the peel, particularly due to cell enlargement in the albedo.[29] These changes are necessary to compensate for the rapid growth of the pulp. Irregularities in the pectin layer of the albedo develop into small protuberances and the pectin layer gives the cells a regular shape.[29] Hydrophilic colloids in the cell walls have a high importance for the transport of substances into the pulp of citrus fruits, where

there is no direct vascular contact between the peel and the developing juice sacs.[30] Finally, the juice sacs enlarge to fill the pulp segments.[29] Thus, as the pulp increases, the peel tissue is compressed in radial direction and it becomes thinner and denser, whereas it is stretched in the tangential direction.

The μCT scans of the fruit peels illustrate the structure of the peel, and especially the structure of the vascular bundles, very clearly (Section 3.2 CT imaging) (ESI†). In addition, no major drying effects could be detected in the images. The total volume of the peel decreased slightly, but the contrast gain compared to fresh samples is enormous. An alternative to prevent even the minimal shrinkage could be an appropriate staining with *e.g.* PTA,[31] which in a preliminary study led to a better visualization of the vascular bundles, but to a significantly weaker visualization of the cellular tissues. The predominate radial orientation of the vascular bundles from pulp to epidermis, which primarily serves to transport fluid within the peel, also provides a support function against stresses acting on the peel from outside due to the increasingly denser arrangement of vascular bundles towards the pulp.[5,32] It can be hypothesized that a local impact applied to the peel from the outside is distributed globally throughout the entire peel so that the stresses are distributed in the peel as homogeneously as possible. In this way, the system of vascular bundles contributes to a homogeneous load distribution and prevents stress peaks that could damage the peel.

The SEM images clearly visualize the differences of the cells and cellular structure of the two tissue types (flavedo and albedo) (Section 3.3 SEM imaging) regarding cell shape and arrangement. While the outer flavedo is mainly suited to prevent penetration and to distribute stresses more globally comparable to the top layer of a sandwich structure,[2] the inner albedo is much more suited to dissipate stresses by compressing the less dense tissue and thus to protect the pulp and the seeds from damage after impacting on the soil.[2] Other studies on citrus fruit peels show that the graded transition between albedo and flavedo is essential and compare it to a functionally graded material (FGM).[2] It can be hypothesized that stresses run out in the cavities, *i.e.* the intercellular spaces. In addition, the intercellular spaces provide a expansion space for the cells that are pressed into the intercellular spaces during compression. This protects the cells from damage due to compression, as they would burst if they had no space to deform.

To determine the proportion of intercellular spaces in the peel, thin sections were analyzed both manually and with the software ilastik (Section 3.4 Intercellular spaces of the peel of *Citrus* spp.). Comparison of the same thin sections with the two evaluation methods shows no significant difference ($p > 0.05$) in the proportion of intercellular spaces in the fruit peel. Since a data set could be evaluated several times faster with ilastik without resulting in a significant difference of the data sets, it clearly argues for the use of the software. Although first-time handling of the software ilastik can be time-intensive, thereafter an entire data set can be analyzed in a short time and the process is very time-efficient. With a data set of 10 images, approx. 30% of the time required for a manual segmentation was needed.

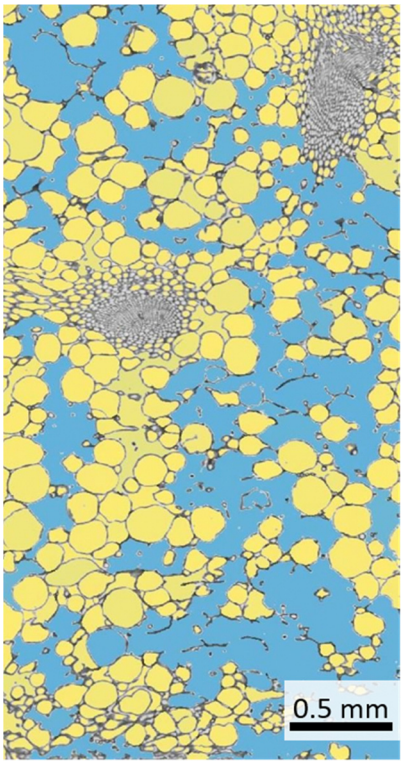

Fig. 6 Segmentation of cells and intercellular space of a lemon peel thin section using ilastik software. The blue area is segmented intercellular space, whereas the yellow areas are detected cells.

The use of ilastik is widely intuitive and the user gets real-time feedback on the set parameters. The manual evaluation is at least partly subjective and especially with long evaluation times errors can occur. However, the evaluation with the help of the ilastik software is not perfect (Fig. 6). For example, ambiguous areas (*e.g.* damaged cells) are partly not or wrongly detected as intercellular spaces by the software. In spite of that, this can be improved by a longer training phase of the software.

Decisively, the result using the ilastik software is neither better nor worse, but primarily faster and more time-efficient, which is why we recommend the use of the open source project ilastik in this study. For this reason, the data sets of all four citrus species were measured using the software and the intercellular spaces were determined (Fig. 5B). The high percentage of intercellular spaces of pomelo (49.65%) and citron (43.72%) is also reflected in the low densities of the peels. In addition, a low relative flavedo proportion results in a high albedo proportion in the peel, which is characterized by the less densely packed cell tissue. Compression experiments on citrus peels have demonstrated that especially the albedo with its intercellular spaces leads to very low and partly negative lateral contractions (Poisson ratios), which results in excellent impact damping and the associated protection of the pulp and the seeds inside.[3,6,7] Previous studies already highlighted the differences of the tissues.[3,5,6,29] A quantitative determination of the intercellular spaces, a statement about the gradation of the

tissues in terms of stress and impact damping can be made to finally provide a specific model for technical material systems with excellent stress damping and energy dissipating properties.

5. Conclusions

In this study, the structural composition of the peel of lime, lemon, citron and pomelo could be visualized and analyzed. Moreover, the macroscopic differences in peel thickness, density and flavedo proportion between species are also reflected in the proportion of intercellular spaces. Using μCT scans is excellent for illustrating the oil glands and the distribution of the vascular bundles. Moreover, SEM images can be used for structural imaging of the tissue. In this study, it was also possible to quantitatively analyze a large number of thin sections of the peel efficiently and rapidly using the ilastik software, without any significant difference compared to much more time expensive manual analysis. The large number of intercellular spaces in the albedo but also the denser flavedo both have a protective function. While the flavedo rather protects against penetration, the albedo primarily dissipates energy due to the low lateral compression. In addition, the entire peel structure is mechanically supported by vascular bundles, the citrus peel can also be called a functional grade material (FGM) with vascular bundle reinforcement which due to its 3D-arrangement also helps for distributing strains and stresses.

In conclusion, it should be noted that all the citrus fruit peels examined show only minimal differences in the orientation of the vascular bundles. This is an indication that – as hypothesized – the vascular bundles in all species examined play an important role in distributing the locally acting mechanical stresses, which occur *e.g.* when a fruit impacts on the soil, globally throughout the entire peel. Differences in the damping properties between different citrus species are mainly due to variations in the graded peel structure and the peel thickness. The intercellular spaces, which also exist in all species tested, serve to prevent the cells from bursting when the fruit is compressed by allowing for deformation of the cells into the intercellular spaces. In addition, the grading of the cellular structure is accompanied by a minimization of the lateral expansion of the peels under axial compression. This material behavior is also referred to as auxetic. An auxetic material behavior or at least a very low lateral expansion has been demonstrated in various citrus fruit peels.[7]

This combination of penetration protection, impact and energy dissipation makes *Citrus* spp. peels a promising idea generator for technical material systems.

Data availability

The data is available upon reasonable request.

Author contributions

TS supervised and initiated the study, and acquired the funding. MJ, VA & TK carried out data collection, data assessment and the statistical analyses. Data evaluation and discussion of the results was a joint effort of all authors (MJ, VA, TK, TS). MJ wrote the first draft of the manuscript, MJ & TS worked on the final draft of the manuscript. All authors gave final approval for publication.

Conflicts of interest

The authors declare that they have no known competing financial interest or personal relationships that could have appeared to influence the work reported in this paper. The funders had no role in the design of the study; in the collection, analyses, or interpretation of data; in the writing of the manuscript; or in the decision to publish the results.

Acknowledgements

This research was funded by the Excellence Cluster livMatS (funded by the Deutsche Forschungsgemeinschaft (German Research Foundation, DFG) under Germany's Excellence Strategy – EXC-2193/1 – 390951807). The publication was paid for by open access agreement – Albert-Ludwigs-Universität Freiburg.

References

1 M. Thielen, T. Speck and R. Seidel, Impact behaviour of freeze-dried and fresh pomelo (*Citrus maxima*) peel: influence of the hydration state, *R. Soc. Open Sci.*, 2015, 140322, DOI: 10.1098/rsos.140322.

2 M. Jentzsch, S. Becker, M. Thielen and T. Speck, Functional Anatomy, Impact Behavior and Energy Dissipation of the Peel of *Citrus* x *limon*: A Comparison of *Citrus* x *limon* and *Citrus maxima*, *Plants*, 2022, **11**, 991, DOI: 10.3390/plants11070991.

3 B. Yang, W. Chen, R. Xin, X. Zhou, D. Tan, C. Ding, Y. Wu, L. Yin, C. Chen and S. Wang, *et al.*, Pomelo Peel-Inspired 3D-Printed Porous Structure for Efficient Absorption of Compressive Strain Energy, *J. Bionic Eng.*, 2022, **19**, 448–457, DOI: 10.1007/s42235-021-00145-1.

4 Z. Zhang, A. Olah and E. Baer, Mechanical compressive behavior of pomelo peel and multilayer polymeric film/foam systems, *Bioinspiration Biomimetics*, 2022, **17**(5), 056004, DOI: 10.1088/1748-3190/ac7d29.

5 M. Thielen, C. N. Z. Schmitt, S. Eckert, T. Speck and R. Seidel, Structure-function relationship of the foam-like pomelo peel (*Citrus maxima*)-an inspiration for the development of biomimetic damping materials with high energy dissipation, *Bioinspiration Biomimetics*, 2013, **8**, 25001, DOI: 10.1088/1748-3182/8/2/025001.

6 B. Wang, B. Pan and G. Lubineau, Morphological evolution and internal strain mapping of pomelo peel using X-ray computed tomography and digital volume correlation, *Mater. Des.*, 2018, **137**, 305–315, DOI: 10.1016/j.matdes.2017.10.038.

7 M. Jentzsch, M.-C. Badstöber, F. Umlas and T. Speck, Damage protection in fruits: Comparative analysis of the functional morphology of the fruit peels of five Citrus

species *via* quasi-static compression tests, *Front. Mater.*, 2022, **9**, 979151, DOI: 10.3389/fmats.2022.979151.
8 M. Thielen, T. Speck and R. Seidel, Viscoelasticity and compaction behaviour of the foam-like pomelo (*Citrus maxima*) peel, *J. Mater. Sci.*, 2013, **48**, 3469–3478, DOI: 10.1007/s10853-013-7137-8.
9 S. F. Fischer, M. Thielen, R. R. Loprang, R. Seidel, C. Fleck, T. Speck and A. Bührig-Polaczek, Pummelos as Concept Generators for Biomimetically Inspired Low Weight Structures with Excellent Damping Properties, *Adv. Eng. Mater.*, 2010, **12**, B658–B663, DOI: 10.1002/adem.201080065.
10 A. Bührig-Polaczek, C. Fleck, T. Speck, P. Schüler, S. F. Fischer, M. Caliaro and M. Thielen, Biomimetic cellular metals-using hierarchical structuring for energy absorption, *Bioinspiration Biomimetics*, 2016, **11**, 45002, DOI: 10.1088/1748-3190/11/4/045002.
11 T.-T. Li, H. Wang, S.-Y. Huang, C.-W. Lou and J.-H. Lin, Bioinspired foam composites resembling pomelo peel: Structural design and compressive, bursting and cushioning properties, *Composites, Part B*, 2019, **172**, 290–298, DOI: 10.1016/j.compositesb.2019.04.046.
12 E. S. Ford, Anatomy and Histology of the Eureka Lemon, *Bot. Gaz.*, 1942, 288–305, DOI: 10.1086/335133.
13 F. M. Scott and K. C. Baker, Anatomy of Washington Navel Orange Rind in Relation to Water Spot, *Bot. Gaz.*, 1947, 459–475, DOI: 10.1086/335434.
14 P. Klock, M. Klock and T. A. Klock, *Das große Ulmer-Buch der Zitruspflanzen*, Ulmer, Stuttgart, 2007, ISBN 9783800146932.
15 M. S. Ladaniya, *Citrus fruit: Biology, technology and evaluation*, Elsevier Academic Press, ScienceDirect: Amsterdam, Heidelberg, Amsterdam, 2008, ISBN 9780123741301.
16 S. Dhondt, H. Vanhaeren, D. van Loo, V. Cnudde and D. Inzé, Plant structure visualization by high-resolution X-ray computed tomography, *Trends Plant Sci.*, 2010, **15**, 419–422, DOI: 10.1016/j.tplants.2010.05.002.
17 L. Hesse, K. Bunk, J. Leupold, T. Speck and T. Masselter, Structural and functional imaging of large and opaque plant specimens, *J. Exp. Bot.*, 2019, **70**, 3659–3678, DOI: 10.1093/jxb/erz186.
18 C. Sommer, C. Straehle, U. Kothe and F. A. Hamprecht, Ilastik: Interactive learning and segmentation toolkit, IEEE International Symposium 032011, 2011, pp. 230–233, ISBN 978-1-4244-4127-3.
19 I. Arganda-Carreras, V. Kaynig, C. Rueden, K. W. Eliceiri, J. Schindelin, A. Cardona and H. Sebastian Seung, Trainable Weka Segmentation: a machine learning tool for microscopy pixel classification, *Bioinformatics*, 2017, **33**, 2424–2426, DOI: 10.1093/bioinformatics/btx180.
20 I. Luengo, M. C. Darrow, M. C. Spink, Y. Sun, W. Dai, C. Y. He, W. Chiu, T. Pridmore, A. W. Ashton and E. M. H. Duke, *et al.*, SuRVoS: Super-Region Volume Segmentation workbench, *J. Struct. Biol.*, 2017, **198**, 43–53, DOI: 10.1016/j.jsb.2017.02.007.
21 O. Hilsenbeck, M. Schwarzfischer, D. Loeffler, S. Dimopoulos, S. Hastreiter, C. Marr, F. J. Theis and T. Schroeder, fastER: a user-friendly tool for ultrafast and robust cell segmentation in large-scale microscopy, *Bioinformatics*, 2017, **33**, 2020–2028, DOI: 10.1093/bioinformatics/btx107.
22 S. Berg, D. Kutra, T. Kroeger, C. N. Straehle, B. X. Kausler, C. Haubold, M. Schiegg, J. Ales, T. Beier and M. Rudy, *et al.*, ilastik: interactive machine learning for (bio)image analysis, *Nat. Methods*, 2019, **16**, 1226–1232, DOI: 10.1038/s41592-019-0582-9.
23 L. Breiman, Random Forests, *Mach. Learn.*, 2001, **45**, 5–32, DOI: 10.1023/A:1010933404324.
24 C. Sommer, L. Fiaschi, F. A. Hamprecht and D. Gerlich, ICPR 2012: The 21th International Conference on Pattern Recognition, November 11–15, 2012, Tsukuba, Japan, IEEE Computer Society, 2012, ISBN 9784990644116.
25 Y. M. Staedler, D. Masson and J. Schönenberger, Plant tissues in 3D via X-ray tomography: simple contrasting methods allow high resolution imaging, *PLoS One*, 2013, **8**, e75295, DOI: 10.1371/journal.pone.0075295.
26 R Core Team. R; R Foundation for Statistical Computing, Vienna, Austria, 2019.
27 E. Stover, W. Castle and C.-C. T. Chao, Trends in U.S. Sweet Orange, Grapefruit, and Mandarin-type Cultivars, *HortTechnology*, 2005, **15**, 501–506, DOI: 10.21273/HORTTECH.15.3.0501.
28 A. Abouzari and N. Mahdi Nezhad, The Investigation of Citrus Fruit Quality. Popular Characteristic and Breeding, *Acta Univ. Agric. Silvic. Mendel. Brun.*, 2016, **64**, 725–740, DOI: 10.11118/actaun201664030725.
29 J. M. Bain, Morphological, anatomical, and physiological changes in the developing fruit of the Valencia orange, Citrus sinensis (L) Osbeck, *Aust. J. Bot.*, 1958, **6**, 1, DOI: 10.1071/BT9580001.
30 H. S. Reed, The swelling of citrus fruits, *Am. J. Bot.*, 1930, 971–982, DOI: 10.1002/j.1537-2197.1930.tb04934.x.
31 A. S. Westermeier, N. Hiss, T. Speck and S. Poppinga, Functional-morphological analyses of the delicate snap-traps of the aquatic carnivorous waterwheel plant (Aldrovanda vesiculosa) with 2D and 3D imaging techniques, *Ann. Bot.*, 2020, **126**, 1099–1107, DOI: 10.1093/aob/mcaa135.
32 K. J. Niklas, *Plant biomechanics: An engineering approach to plant form and function*, Univ. of Chicago Press, Chicago, Ill, 1992, ISBN 0226586308.